

# Ab initio informed machine learning potential for tribochemistry and mechanochemistry: Application for eco-friendly gallate lubricant additive

Huong T.T. Ta<sup>a</sup>, Mauro Ferrario<sup>a,b</sup>, Sophie Loehlé<sup>c</sup>, M. Clelia Righi<sup>a,\*</sup>

<sup>a</sup> Department of Physics and Astronomy, University of Bologna, Bologna 40127, Italy

<sup>b</sup> FIM Department, University of Modena and Reggio E, Modena 41125, Italy

<sup>c</sup> TotalEnergies, OneTech Fuels&Lubricants, Research Center Solaize, Solaize 69360, France

## ARTICLE INFO

### Keywords:

Tribochemistry  
Active learning  
Ab-initio calculations  
Deep neural network  
Friction and wear  
Molecular dynamics

## ABSTRACT

Mechanochemistry and tribochemistry processes involve multiple physical/chemical interactions induced by extreme conditions including molecular confinement, high temperatures and mechanical stress applied. Simulating these processes by molecular dynamics is very challenging. While force fields fall short reproducing the enhanced reactivity arising by quantum effects, *ab initio* molecular dynamics is severely limited by the complexity of the systems of interest, their sizes, and the long-time scale on which relevant events take place. In this work using an active learning approach, a landmark deep neural network potential has been developed which reproduces the accuracy of *ab initio* interactions at the classical molecular dynamics computational cost and permits to successfully simulate the tribochemical processes occurring at the interface between butyl gallate molecules and iron substrates under tribological conditions. The simulations of the dynamics of the Fe-gallate system when sliding under an imposed external load reveal the key atomistic mechanisms underlying the formation of the friction reducing lubricant tribofilm and permit to characterize the tribological properties of the explored systems, clearly exposing the shortcoming of reactive force field based approaches. The successful development of neural network potentials, making it possible to push the limits of molecular dynamics marrying accuracy with system sizes and long time scales, paves the route toward a new area in computational tribochemistry.

## 1. Introduction

Mechanochemistry and tribochemistry are the terms that have been widely used in recent decades to refer to the chemical transformation activated by mechanical forces applied to the system. [1] While the term mechanochemistry is a general description of mechanically induced chemical reactions, a more specific term – tribochemistry – was introduced later to denote the physico-chemical alterations experienced at the solid–solid or solid–liquid interfaces during tribological processes. Such alterations have a high impact on friction, wear and lubrication of solids. [1,2] These phenomena are ubiquitous in our daily life, from human biological organs [3] to nano/micro-electromechanical systems, [4,5] automotive, [6] manufacturing, [7] and aerospace industries. [8,9] In accordance with its long history and widespread applications, scientists are ever trying to understand fundamental mechanisms governing these events with an ultimate target of

controlling adhesion, friction, wear, improving the energy efficiency and minimizing manufacturing/maintenance costs. However, a typical tribomechanical process may involve several fundamental steps from mechanical to physical and chemical transformation, governed by many parameters such as the surface reactivity, the working stresses and temperatures, the interaction with lubricant and environmental molecules. The extreme conditions ruling tribochemistry and mechanochemistry processes play a key role to initiate reactions and drive the formation of the lubricating tribofilms. [2,10] These combinations pose the greatest challenge for real-time experiments. Atomic scale insight provided by computer simulations is a powerful tool that play an essential role in fruitfully accessing information on kinetics, thermodynamics and statistics of mechanochemical and tribochemical events *in situ*.

Targeting on tribo-induced chemical reactions, the essential role of tribochemical simulations stands or falls by the capability of describing

\* Corresponding author.

E-mail address: [clelia.righi@unibo.it](mailto:clelia.righi@unibo.it) (M.C. Righi).

bond forming and breaking events under harsh dynamics conditions. Several atomistic simulation methods across scales from quantum mechanics to classical *molecular dynamics* (MD) have been applied to access detailed information from mechanochemical and tribochemical reactions. [11,12] However current atomistic tribochemical simulations stand in between an accuracy versus efficiency dilemma. In fact, at the atomic scale, *ab initio molecular dynamics* (AIMD) allows for an accurate description of charge transfer and related chemical processes. AIMD has been successfully used to describe tribochemical reactions between a variety of lubricant molecules and substrates such as metals, [13] oxides, [14–17] diamond, [18–20] silicates, [19,21] etc. The main outcome of AIMD is to provide insights into local chemical events, particularly on bond formation and breaking under harsh conditions. [14–16,19] However, the expensive computational costs set a modest limit for AIMD system sizes and simulation time scales. So far, it is still impractical to apply AIMD method beyond small-scale reactive systems of tribology, in particular for steel surfaces due to the increased computational efforts required to properly describe iron at the quantum level. Obtaining atomic-scale insights from larger scale models still rely on MD simulations with interaction described by alternative *force fields* (FF), e.g. using empirical [22,23] or reactive FFs. [24–29] The choice of empirical FFs seemingly solves all issues with the simulation scales yet leaves out biggest concerns regarding its accuracy and reliability. Instead, reactive FFs such as adaptive intermolecular reactive empirical bond order (AIREBO), charge optimized many body (COMB), or ReaxFF are considered a more suitable alternative since bond order is taken into account with a bearable increase in the computational costs. However, the lack of inter-atomic potentials and transferability for complex tribological systems progressively limit the applications of ReaxFF MD [26]. [30,31] Furthermore, the reactivity of molecules in harsh tribochemical conditions is augmented by quantum effects that cannot be properly included and reproduced within the constraints of these FF parametrizations.

Recently, machine learning (ML) based potentials have been intensively developed, [32–35] signifying a new prototype of atomistic simulations in the last few years. ML potentials are developed based on the data from high accurate quantum chemical methods such as DFT based on two most common approaches: high-dimensional neural networks (NN) and kernel-based methods. A proper-trained potential, therefore, inherits the accuracy of quantum mechanics level with the cost of classical simulations, which consequently addresses the question of the accuracy and efficiency trade-off. The development of ML has heralded the onset ML technology in atomistic simulations and achieved unprecedented level of description for the dynamics of a variety of material categories ranging from metallic bulk, [36–39] organic molecules, [40,41] and particularly more complex systems such as surfaces/interfaces. [42–47] Recent successful applications of ML potentials on describing surface/interface systems include proton transfer at TiO<sub>2</sub> and GaP(110)–water interfaces, [42,44,47] acid dissociations at air–water interfaces, [45] or thermal transport across copper–water interface. [43] These examples manifest the capability of ML potentials for describing physical/chemical phenomena in complex interfacial systems.

Despite the successes of ML methods in atomistic simulations in many fields, to the best of our knowledge, no ML-based molecular dynamics simulations have been published with a study of chemical reactions in the fields of tribochemistry or mechanochemistry. This is due to the fact that unlike homogenous systems, the training of a ML potential for tribological model is not a trivial task. The difficulties of training a proper potential for tribochemistry arise from the complex reaction paths of tribological systems and unconventional mechanism of activation in a dynamic environment driven by multiple concurrent factors. [2,10]

In this work, we present the protocol adopted to train a NN based potential for tribochemical systems from the data obtained from *ab initio* calculations. We will from now on refer to this model as BG-

DNN15. The process includes the data generation, training, active learning approach, and validation to build reliable potentials for atomistic simulations of tribochemistry. Specially, we applied the method for constructing a ML-based model to study the friction reduction mechanisms of gallate molecules, a new class of green lubricant additives [48] that include one aromatic ring with hydrocarbon chains of different length. These compounds are being experimentally tested for their properties in reducing friction coefficients and wear rates thanks to their ability to form lubricious self-assembled monolayers (SAM). Butyl gallate (BG) with a chain of 4 C atoms was selected in this work as representative of the gallate molecule group and the Fe (110) surface was used as the metal substrate as locally it may represent the native steel surface often exposed in experimental tribo-tests. [49]

The paper is organized as follows. In the section **Results** “**Adsorption of butyl gallate molecules on the Fe (110) surface**” we begin describing by *ab-initio* DFT calculations the adsorption of BG molecules on the iron surface, then detail the structures implemented in the training database and the implementation of training with an active learning procedure in the section **Results** “**Data Generation and Training of the BG-DNN15 potential model**”. The validation of the ML potential model is detailed in the section **Results** “**Training Results and Validation of the BG-DNN15 potential model**” and then we assess its qualities and merits by comparison with AIMD simulations in the section **Results** “**Validation in tribological conditions**”, highlighting the shortcomings of ReaxFF potential model when used under harsh conditions. Finally applying the trained NN potential model we predict how the butyl gallate self-assembled monolayer reduces friction at the Fe-Fe interface in the section **Results** “**Tribological properties calculated by DPMD simulations**”. In the section “**Discussion**” the tribochemical reactions and their role in the setup and stability under increasing load of the lubricious butyl gallate self-assembled monolayer are critically reviewed and we conclude by outlining further research directions to be explored with the help of the BG-DNN15 potential.

## 2. Methods

### 2.1. *Ab initio* calculations for data production

The *ab initio* calculations were performed using spin-polarized density functional theory (DFT) implemented in VASP package version 6.3.2. [50] The projector-augmented wave (PAW) method was used for the interaction between electrons and ions. The exchange and correlation functional was described by the general gradient approximation (GGA) with the Perdew–Burke–Ernzerhof (PBE). [51] The convergence threshold of the electronic self-consistent (SCF) loop were set at 10<sup>−5</sup> eV. Brillouin zone was sampled at the gamma point and the plane-wave expansion of the electronic wave function was truncated by setting the cutoff energy to 450 eV. The DFT–D2 method of Grimme [52,53] was adopted to account for the Van der Waals (vdW) dispersion interactions between aromatic molecules.

To generate the initial data set used for the training of the initial ML potential, configurations were generated by means of AIMD simulations performed in the NVT ensemble at different temperatures of 300 K, 500 K, 1000 K, 2000 K, and 3000 K, with a timestep of 1.0 fs used to integrate the equations of motion. The systems were equilibrated at the given temperatures over a period of time of ~3 ps. Energies and forces from all configurations extracted from the AIMD simulations were further refined by performing additional SCF calculations.

### 2.2. *Ab initio* molecular dynamics in tribological conditions

To perform the AIMD simulations under tribological conditions we used a modified version of the Quantum Espresso package [57,58] which allows to impose at the interface a lateral sliding at constant velocity while removing excess heat to control the substrate temperature. The code has been successfully used for studying the

tribochemistry of different systems, including metal–lubricant interfaces. [21] The electronic parameters were set to be equivalent to those used in the DFT and AIMD simulations with VASP, with ultrasoft pseudopotentials used to describe the core electrons of the system. The GGA with PBE [51] method was used as the exchange–correlation functional. The plane–wave basis set was used to expand the electronic wave function with cutoff energies of 30 Ry for the wave function and 240 Ry for the charge density, respectively. The gamma point was used for the Brillouin zone sampling. The semi–empirical correction by Grimme (D2) [52,53] was adopted to account for the vdW dispersion interactions between aromatic molecules. The Verlet algorithm with a timestep of 20 a.u. ( $\sim 1$  fs) was used to integrate the movement of atoms in the system. An external force corresponding to a typical tribological load of 1 GPa was applied along the  $z$ -direction and a constant temperature of 300 K was imposed to the iron substrates. During the sliding the system was first equilibrated 1 ps with the topmost layer of the upper iron slab moved along the  $X$  direction with a constant velocity of 200 m/s with respect to bottom-most layer of the lower iron slab. The simulations were then carried on for further duration of 5 ps. More details about the simulation of sliding using the modified Quantum Espresso code can be found in our previous publications. [20,54]

### 2.3. Molecular dynamics simulations

For the system of 6 BG molecules confined between two Fe substrates, simulations with imposed sliding under a 1 GPa load were performed at a constant temperature of 300 K with Lammmps [55] using the ReaxFF force field of Shin *et al.* [56] The MD simulations were performed with a timestep of 0.05 fs for as long as 100 ps, with structures extracted at every 1 ps to be selected as candidate configurations to be included in the initial data set for the training. Further details about the setting of the MD simulations with ReaxFF can be found in [Supporting Information](#).

Molecular dynamics simulations with the BG-DNN15 potential model were performed with Lammmps [55] at different applied loads ranging from 0.5 GPa to 2 GPa, in the NVT ensemble at 300 K using separate Nosé–Hoover thermostats for each of the iron slabs. Tribological conditions were simulated imposing a fixed relative velocity between the uppermost and the bottom-most layer of iron atoms. All calculations were performed with a time step of 0.1 fs to ensure a correct integration of the atomic trajectories in the strong repulsive force region. This, together with our specific active learning sampling, was sufficient to avoid the insurgence, particularly while simulating under imposed sliding, of unphysical configurations due to known shortcomings of ML-based methods in describing very short-distance interactions without having to resort to additional empirical terms. [57] During the simulations, the atomic configurations of the system were collected at every 10 fs along the trajectories obtained from the DPMD runs.

### 2.4. Training of the potential model with deepMD-kit

The ML potential was trained using the DeepMD–kit package with the DeepPot–SE (Deep Potential–Smooth Edition) model. [35] The package is written in the Python/C++ languages interfaced with TensorFlow [58] to perform the neural network training based on evaluation of atomic energies and forces. The model includes two networks, i.e., the embedding network and the fitting network. The size of the embedding network was set to (25, 50, 100), and the size of the fitting network was set to (240, 240, 240). The cutoff radius was set to 6.0 Å, and the descriptors decayed smoothly from 0.5 to 7.0 Å. The initial learning rate was set to 0.001 at the beginning of the training process to achieve a final value of  $1 \times 10^{-8}$ . The total numbers of training batches are  $1 \times 10^6$  for the training in the initial iterations and the active learning process and  $1.5 \times 10^6$  for the production of the final model.

To effectively improve the ML potential, additional data was generated through an active learning approach as proposed by Zhang *et al.* [59] At each iteration, four models were trained using the same input setups but starting with different random seeds. To explore new configurations to enrich the data sets, deep potential molecular dynamics simulations were performed with the first model taken as reference, collecting the atomic configurations of the system at every 10 fs along the obtained trajectories. The DPMD simulations were performed under sliding condition for a duration of  $\sim 10$ –125 ps after a short equilibrium of 10 ps under the loads of 0.5, 1.0, 1.5, and 2.0 GPa at 300 K. During the DPMD simulations, the force acting on each atom at the collected configurations was evaluated by all four models. The maximum standard deviation of the atomic forces ( $\sigma_f^{\max}$ ) was evaluated as a criterion for the convergence of the neural network training:

$$\sigma_f^{\max} = \max_i \sqrt{\|f_i - \langle f_i \rangle\|^2} \quad (1)$$

where,  $f_i$  is the force acting in atom  $i^{\text{th}}$ ,  $\langle f_i \rangle$  is the average value taken from four models. A structure is considered as a candidate if the maximum standard deviation falls in the range of  $\sigma_f^{\text{low}} < \sigma_f^{\max} < \sigma_f^{\text{high}}$ , while those with  $\sigma_f^{\max} < \sigma_f^{\text{low}}$  are considered correct structures, and those with  $\sigma_f^{\max} > \sigma_f^{\text{high}}$  can be highly unphysical configurations and classified as failed structures. The satisfied candidates taken from the sliding processes were selected and subjected to DFT calculations to obtain the energies and forces and included into the data sets. The training with new four models was repeated until a very small portion of structures are identified as candidates. Due to the complexity of the interfacial and sliding systems and extreme condition simulations, the forces exerted in the systems are also high. Thus, in our work, the candidates were selected if  $\sigma_f^{\max}$  is in between  $0.15 < \sigma_f^{\max} < 0.5$ . The lower threshold is a typical value to select candidates in active learning method, [44,46] while the upper value is set to be as high as 0.5 considering the high absolute values of forces sampled from OH bond stretching. Under tribological condition, more untrained configurations were explored as the simulation time gets longer, and the typical DPMD run of 10–20 ps is not sufficiently long to make sure that the candidates are enough representatives. Thus in the last 2 iterations, longer DPMD runs of 125 ps were performed, and only the configuration with the highest  $\sigma_f^{\max}$  at every 200 fs was considered as the candidate. This approach resulted very effective in reducing the number of highly correlated configurations and allowed sampling new representative candidates that permitted to obtain stable MD runs for as long times as required.

Since this active learning process focused on the improvement of the interfacial interaction between the iron surface and the BG molecules, to reduce the computational cost from the Fe substrates, the two outermost layers of each Fe slab of the selected candidates were removed for the DFT calculations of energies and forces. The reduced system still includes enough chemical components to fully represent the atomic environments for Fe–BG sliding models.

## 3. Results

### 3.1. Adsorption of butyl gallate molecules on the Fe (110) surface by first principles

The interaction between the BG molecule and the iron surface is a complex function of the molecular orientation and coverage, with significant differences in the behavior of the isolated molecule compared with ordered structure of the self-assembled monolayer. The characterization of the adsorption of the BG molecules on the Fe (110) surface was performed by first-principles calculations, in order to provide us with some initial idea about favorable adsorption sites and relevant geometries to be adopted in building the ML models.

First, one BG molecule was positioned in a supercell, with lateral dimensions  $14.20 \times 12.05 \text{ Å}^2$ , on the Fe (110) surface at different adsorption sites and molecular orientations (perpendicular and parallel). For such a low coverage, the most stable configuration is given by the



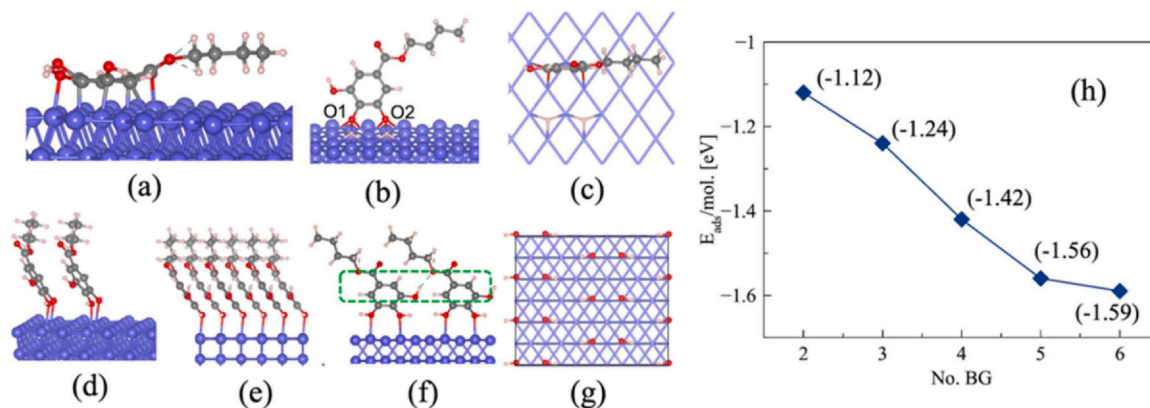


**Fig. 1.** Geometrical optimization of BG adsorption on the Fe (110) surface: side (a) view of one BG molecule, side (b) and top (c) views of dissociative adsorption of one BG molecules, side (d) view for two BG molecules and side (e-f) views for six BG molecules adsorbed on the Fe (110) surface, (g) top view of the oxygen chemisorption sites at the highest molecular coverage. (h) adsorption energy per molecule ( $E_{ads}/mol$ ) as a function of coverage. The dotted green box in (f) marks the region where inter-molecular hydrogen bonding occurs. Only the oxygen atoms bonded to the Fe surface of the molecules are visualized in (g). Color assignment applied throughout this work: Fe (blue), C (gray), O (red), and H (light pink).

*parallel* orientation to the surface, i.e. the one with the atoms of the carbon ring on top of Fe atoms (Fig. 1a), which has a corresponding adsorption energy of  $-3.90$  eV. This configuration maximizes chemical bonding between the surface and the atoms of the molecule, i.e. the number of Fe–O and Fe–C contacts, while the atoms in the hydrocarbon tail only contribute through their short-range van der Waals interactions. The Fe–C and Fe–O bond lengths range from  $1.96$  Å to  $2.20$  Å, which are well inside the range of strong chemical interaction. As a result, the aromatic ring is distorted, while the physical interaction keeps the hydrocarbon tail intact at  $\sim 3.2$  Å –  $3.4$  Å from the iron surface. Even when trying to start a single BG molecule adsorption with an initial *perpendicular* orientation, the optimization ends up with the molecule down in the *parallel* configuration, similar to the previous case but in different, slightly higher, minima. Interestingly, we found that we could obtain a local minimum with the *perpendicular* configuration for a single BG molecule adsorption at the expense of letting two H atoms detach from the two OH bonds which were closer to the iron surface (Fig. 1b). These H atoms chemisorb independently on the iron surface and the overall adsorption energy for such a process is  $-3.45$  eV, still higher than the lowest one for the *parallel* case with the intact molecule but as we shall see with a non-negligible probability in standard conditions at 300 K. This dissociative adsorption can be stable perpendicularly by forming multiple Fe–O bonds when the O1 and O2 atoms move to the 3-fold (3F) sites of the Fe (110) surface. Similarly, H

atoms are adsorbed at the most favorable 3F sites at the Fe–H distances of  $\sim 1.76$ – $1.79$  Å (Fig. 1b–c). Although, for the single isolated molecule, the *parallel* adsorption of the intact BG molecules remains the most favorable, as the coverage increases the geometrical optimization suggests that stable minima for the *perpendicular* adsorption configuration can be achieved from the co-adsorption of at least two (Fig. 1d) or more BG molecules. The molecules are adsorbed in a stable configuration on the surface by forming Fe–O chemical bonds between topmost adjacent Fe atoms of the surface (Fig. 1d–f) and two of the three oxygen atoms bonded to the C-ring. In the relaxed configuration the hydrogen atoms of the two OH group remain bonded to oxygen, forming Fe–OH–C bridges with Fe–O bond lengths of  $2.20$  –  $2.31$  Å, which are slightly weaker than those found for the *parallel* configuration. The hydrocarbon tails are relatively far from the iron surface and free to stand upright. This *perpendicular* adsorption configuration is also stabilized by the formation of hydrogen bonds between adjacent molecules (Fig. 1f). As the number of BG molecules per  $\text{nm}^2$  increases, the adsorption energy per molecule becomes more negative and reaches a maximum when 6 BG molecules are adsorbed in the given supercell in an ordered fashion (Fig. 1g), corresponding to a coverage of  $3.51$  molecules/ $\text{nm}^2$ . The calculated average adsorption energies per molecule ( $E_{ads}/mol$ ) are shown in Fig. 1h, where one can observe a steadily decrease with increasing number of molecules, from a value ( $E_{ads}/mol$ ) =  $-1.12$  eV with two BG per supercell to a value ( $E_{ads}/mol$ ) =  $-1.59$  eV with six BG

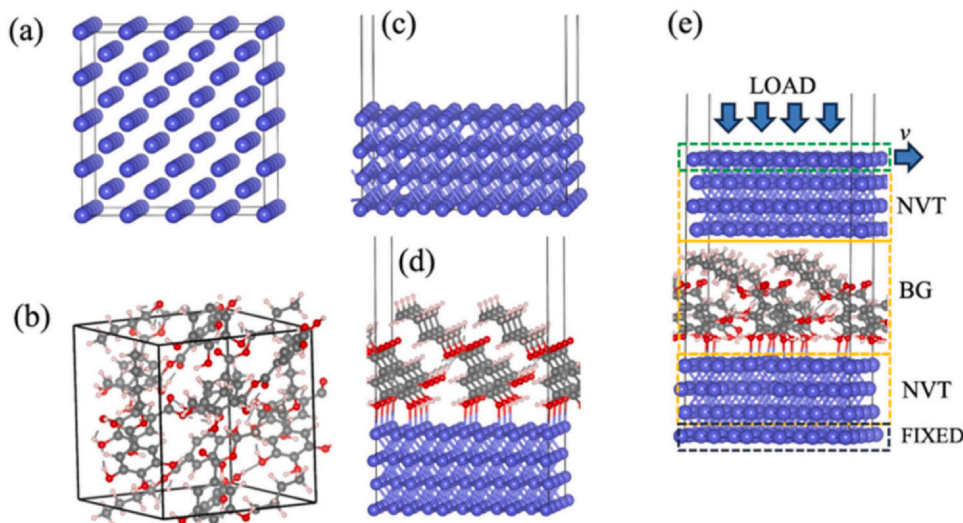


**Fig. 2.** AIMD and MD simulation models for generating the data for the initial NN potential. (a) bulk Fe, (b) 6 BG molecules, (c) Fe (110) surface, (d) 6 BG molecules adsorbed on Fe (110) surface (Fe-6BG<sub>ads</sub>), and (e) model with 6 BG molecules confined in between the two Fe (110) slabs (Fe-6BG) used for molecular dynamics simulations at equilibrium and in tri-biological conditions.

molecules per supercell. This result suggests that when used as lubricant additives we can expect the BG molecules to likely organize themselves in a self-assembled monolayer, which becomes more stable as the surface density of BG molecules gets higher until a maximum coverage of the above given order is reached. Since for the *parallel* stacking of molecules in the given supercell area only the molecule closer to the iron surface can form direct Fe–C and Fe–O, there is no equivalent energy gain with increasing molecular density, and our findings overall confirm that the formation of an ordered BG monolayer is favored in the explored conditions. This is in agreement with the complete match of the XPS signal with the formation of Fe–O–C bridges found experimentally [49] for the adsorption of fatty acids containing two oxygen atoms at the head groups on iron oxide surface. [49,60–62]

### 3.2. Data generation and training of the DNN potential model

The DNN potential was trained using the DeepMD-kit package with the DeepPot-SE (Deep Potential-Smooth Edition) model [35] and to effectively improve the NN potential, additional data was generated through an active learning approach as proposed by Zhang et al. [59] We started the initial training of the NN potential with data generated from short trajectories generated by AIMD simulations for the bulk Fe, the Fe (110) surface, the bulk molecule, and the Fe-6BG interface systems (Fe-6BG<sub>ads</sub>) which are presented in Fig. 2a-d:

- Bulk Fe (Fig. 2a): a  $4 \times 4 \times 4$  supercell containing 128 bcc Fe atoms with experimental density.
- Fe (110) surface (Fig. 2b): a  $3 \times 5$  supercell containing 4 Fe layers, 120 atoms in total.
- Bulk BG (Fig. 2c): 6 molecules (180 atoms) in a cubic box with  $L = 12.76$  Å. The initial configuration and the volume of the system were determined by first running a DFT full relaxation including the cell parameter.
- Fe (110)-6BG<sub>ads</sub> (Fig. 2d): 6 BG molecules perpendicularly adsorbed on the 4 at.-layer Fe (110) surface (300 atoms). The initial orientation of the six BG molecules adsorbed on the Fe (110) surface were determined by the DFT geometrical optimization as previously described.

In order to generate highly diverse structures for the NN training the AIMD simulations were performed at several different temperatures (300 K, 500 K, 1000 K and 2000 K) and at different densities, corresponding to 0.85, 0.9, 1.0, 1.05 times the experimental density for the bulk Fe system or the DFT optimized density for the bulk BG system. The AIMD simulations generated a total of ~55200 configurations.

We were ultimately interested in exploring the tribological properties of the gallates molecules when used as additives to form on the surface a SAM that can play a favorable role in reducing friction and wear between iron surfaces. Therefore, for simulations in tribological conditions we choose as prototype the confined model depicted in Fig. 2e, which is composed by a molecular monolayer that contains six BG molecules (180 C, H and O atoms in total) confined in between two Fe (110) surfaces (Fe-6BG). Each iron slab has a thickness of 4 at.-layers and corresponds to a  $5 \times 3$  supercell containing 120 Fe atoms, resulting in a total number of 420 atoms in the system. The MD simulation of sliding conditions was performed using LAMMPS [55] with the interactions described by a reference ReaxFF force field. [56] The simulation was performed under a 1 GPa load at a temperature of 300 K for 100 ps. The initial configurations for this model were taken from the DFT optimized configurations of the BG molecules adsorbed on the Fe (110) surface. Atomic configurations selected from the generated trajectory at every picosecond were then used to obtain energies and forces at the DFT level, performing static for self-consistent calculations to produce an additional number of ~100 configurations.

### 3.3. Data sampling by active learning method

All the configurations generated from the adsorption study, from the AIMD simulations and from the ReaxFF-driven MD simulations were used to train BG-DNN1, the initial, *first iteration* of the NN model. With the BG-DNN1 potential model a number of ML-driven molecular dynamics (DPMD) simulations were performed for the system described in Fig. 2e, first at the relatively low loads of 0.5 and 1.0 GPa. Due to the limited inclusion of configurations from sliding simulations, the BG-DNN1 model was found to describe very poorly the dynamics under imposed relative sliding of the opposite iron surfaces, resulting, after a time duration of few picoseconds, in a collapse of the system into jammed unphysical structures. Random configurations were selected from the meaningful part of the trajectories produced with a number of attempted DPMD runs, independently started using different initial configurations. The energies and the forces for these selected configurations were then calculated at the DFT level, and these new data structures were added to the training dataset. Repeating the training with the augmented dataset resulted in an improvement of the *second iteration* of the NN potential model, which was then used to perform further DPMD simulations. After iterating this procedure several times, we obtained the BG-DNN8 potential model that was finally able to perform sliding simulations at different pressures for longer time durations, always producing stable structures.

Starting with this latest iteration for the NN potential model we switched to the active learning method [59] using four parallel models to accelerate the learning rate and to improve the quality of the trained model, after further enriching the training dataset with new configurations selected in accordance with the following considerations (see Section **Methods**). The sampled data from the initial AIMD runs and from the DPMD runs in the active learning method mostly fall in or around the local minimum of the chemical reactions and only partially explore the global potential energy surface. In the AIMD simulations at high temperature (1000 – 2000 K), OH bond dissociations occur and the oxygen atom strongly bonds to Fe. This dissociation occurs spontaneously at even lower temperatures for several OH bonds in the systems thanks to the catalytic strength of the iron surface. However, it is worth mentioning that the interpolation in DeepMD-kit can severely underestimate kinetic barriers of chemical reactions. [63] Thus, despite of the good agreement between the predicted data from the NN potential and the *ab initio* data we did find that, under load, the DPMD simulations produced more dissociative events than those observed in the AIMD simulations, probably due to the lack in the training set of sufficient states properly sampling the energy barriers along the transition paths. To improve this situation, starting from the model with 6 BG molecules adsorbed on the Fe (110) surface that corresponds to a total of 12 OH bonds at the interface, as shown in Fig. 2d, we generated an additional set of 1000 artificial structures by applying random displacements to H and O atoms to specifically perturb targeted OH-bonds. In each structure, the OH bonds were randomly stretched from the equilibrium distance to make sure to sample structures different enough from the nearest local minima. Finally, the corresponding energies and forces were obtained by DFT calculations and added to the training set for BG-DNN10 at the beginning of the 10th iteration.

The active learning process generated a total number of 25300 configurations, making a final number of ~80600 configurations, 90% of which were randomly chosen for the training while the remaining 10% were used for the validation.

### 3.4. Training results and validation of the BG-DNN15 potential model

Root-mean-square errors (RMSEs) of the energy and forces for each structure in the datasets are presented in Figure S1a-b as a function of training steps for the training and for the validation datasets. The results reveal both the RMSEs of the energy and the RMSEs of the forces converge well after  $\sim 1 \times 10^6$  step. The averaged RMSEs estimated

over the last  $5 \times 10^5$  steps of the validation dataset are  $1.91 \times 10^{-3}$  eV for the energy and  $0.088$  eV/Å for the forces, respectively. This indicates that the NN potential model was properly trained with values for the errors typical of surface and interface systems. [43,44] Particularly, we obtained comparable values in the learning curves between the training and the validation sets, which confirms no overfitting experienced during the training. To check the convergence of the four NN models during the active learning process, the distribution of the maximum standard deviations of the predicted atomic forces were estimated. The  $\sigma_f^{\max}$  was estimated from the configurations collected at every 2.5 fs from the DPMD simulations of three main systems including the bulk BG, the bulk Fe, and the Fe-6BG sliding systems for 250 ps using the final version BG-DNN15 potential. For the Fe-6BG systems, the sliding simulations were performed at 300 K at three different load pressures including 0.5, 1.0, and 1.5 GPa. An excellent convergence was obtained for the bulk Fe system with the  $\sigma_f^{\max}$  distributed below  $0.05$  eV/Å, as expected being this a homogenous bulk system for which it is easier to obtain a good agreement among the NNs. For Fe-6BG and bulk BG systems, the  $\sigma_f^{\max}$  is distributed below  $0.6$  eV/Å while the peak of the distribution is  $0.1$  eV/Å (see Figure S1c-d in the Supporting Information). Quantitatively, the percentage of configurations that have  $\sigma_f^{\max} > 0.15$  eV/Å is only 1.78%, indicating a good agreement among the neural networks. This is an impressive result considering the long 250 ps timespan of simulation under harsh conditions for such a complex tribological system.

To better characterize the ability of the BG-DNN15 potential to reproduce the *ab initio* data, the energies and forces predicted by DPMD were individually compared with those obtained from *ab initio* calculations for the bulk Fe, the BG molecules, and the Fe-6BG confined systems. The comparison was performed on validation data which was not included in the training set. [42,43]

As shown in Fig. 3, for both energies and forces RMSEs, the BG-DNN15 potential exhibits excellent agreement with the *ab initio* data in all the investigated systems. Deviations for the energy and the forces (Fig. 3c-d) are mostly distributed from  $-0.005$ – $0.005$  eV for the energy, and within the  $-0.2$ – $0.2$  eV/Å range for the forces, respectively.

Specifically, the average root-mean squared errors of the energy and atomic force components predicted by the BG-DNN15 model with respect to DFT were  $2.8 \times 10^{-3}$  eV/atom and  $9.1 \times 10^{-2}$  eV/Å, respectively. It is worth mentioning that despite the inclusion of OH dissociated configurations in the training datasets results in a very large range of values for the forces, from  $-40$ – $40$  eV/Å, nevertheless, the small error values for forces and energy clearly manifest that the trained NN potential has successfully achieved the required accuracy. [43,44]

### 3.5. Validation in tribological conditions: Effects of load

Extreme tribological conditions are always associated with high loads. To investigate the performance of the BG-DNN15 potential model under loading condition, the system was first subjected to geometrical optimization under typical tribological loads, with values ranging from 0.5 GPa up to 2.0 GPa to explore the behavior of the interfacial distance, one important property that can be measured in computational tribology, useful to assess the lubricant ability to maintain the gap between two sliding surfaces.

The optimized  $\Delta z$  widths of the gap at 0K between the two Fe slabs, estimated as the average vertical separation between the iron atoms of the layer at the two interfaces are presented in Fig. 4. The results reveal that, as expected, such interfacial distance  $\Delta z$  gradually reduces as the applied load increases. Not only the tendencies are qualitatively fully matched when comparing the BG-DNN15 potential and the DFT results, but also their magnitudes are well reproduced. In fact, the differences, ranging from 0.17 to 0.34 Å, between the average values listed in Table 1 correspond to less than 3% of the DFT values.

### 3.6. Validation in tribological conditions: Effects of sliding, comparison of dpmd Vs aimd and reaxff

To fully validate the BG-DNN15 potential in tribological conditions, it is essential to compare the systems under dynamic and loading conditions. We performed sliding simulations for the Fe-6BG system under

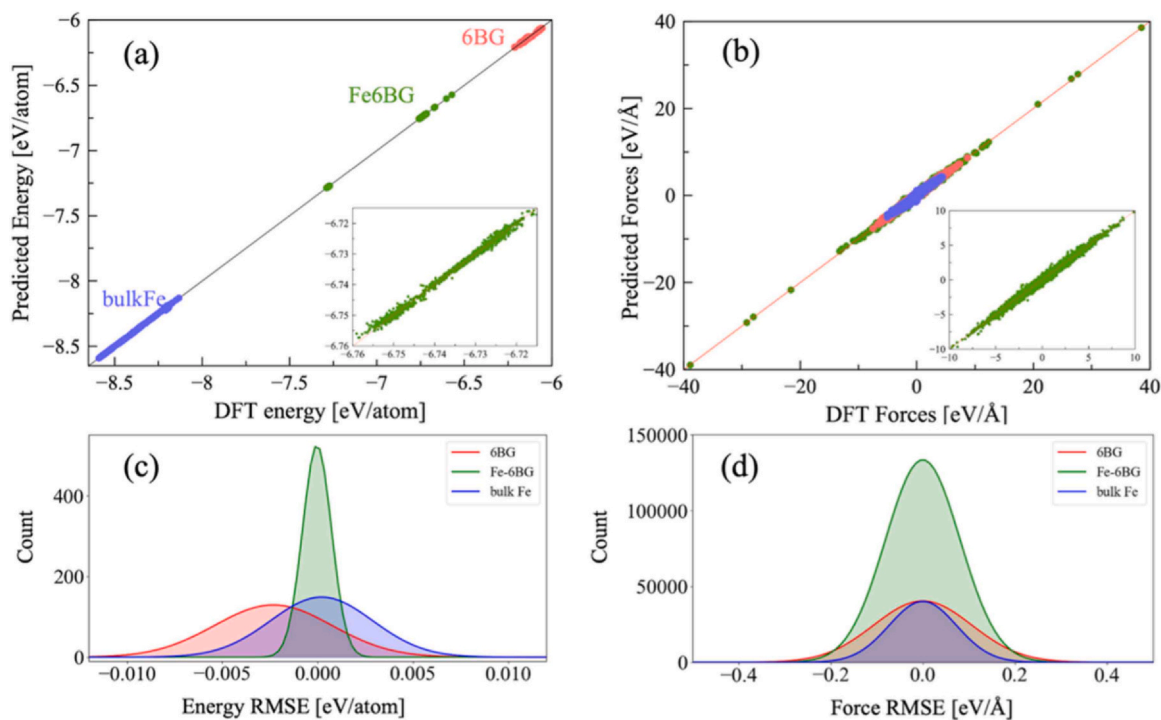


**Fig. 3.** Comparison of the RMSEs for the energy (a) and the forces (b) calculated from the validation data by DPMD and DFT for the three main systems used to train the BG-DNN15 potential. The inserts show the Fe-6BG system on a finer scale. Histogram distribution of the RMSEs between DPMD prediction and DFT calculations for the energy (c) and for the forces (d).



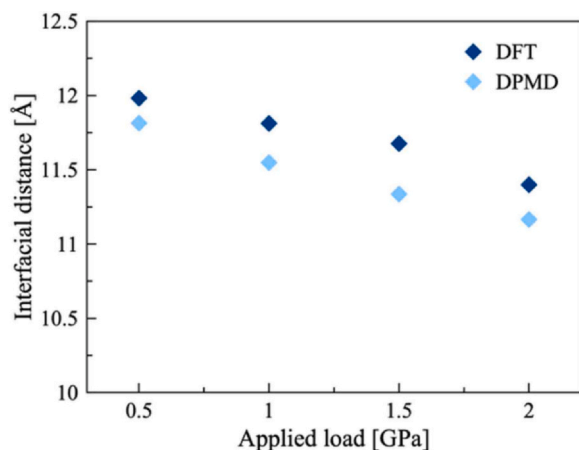


**Fig. 4.** Comparison of the interfacial distance as a function of applied load measured after the geometrical relaxation performed under load, with Quantum Espresso (DFT) and LAMMPS (DPMD).

**Table 1**

Interfacial distances measured after the relaxation of the Fe-6BG model by DFT and DPMD under loads.

Load	0.5 GPa	1.0 GPa	1.5 GPa	2.0 GPa
$\Delta z$ (DFT)	11.98 Å	11.80 Å	11.68 Å	11.39 Å
$\Delta z$ (BG - DNN15)	11.81 Å	11.55 Å	11.34 Å	11.17 Å
Difference	0.17 Å (1.42%)	0.25 Å (2.12%)	0.34 Å (2.99%)	0.22 Å (1.93%)

sliding in tribological conditions (Fig. 2e) by AIMD with a modified version of the Quantum Espresso package [57,58] and repeated them with an identical initial setup by DPMD simulations using the final converged BG-DNN15 potential model with the LAMMPS package [55] interfaced with DeepMD-kit and finally by MD using the reference ReaxFF model [64]. An external force corresponding to a typical tribological load of 1 GPa was applied along the z-direction. The simulations at constant temperature of 300 K included 5 ps of thermalization and 5 ps of sliding starting from the same initial conditions, i.e. same atomic positions and velocities. During the sliding the topmost layer of the iron slab was constrained to move along the positive direction of the x-axis with a constant velocity of 200 m/s. The results were collected and used as the reference for the validation of the NN potential.

In Fig. 5 we show that both the interfacial distances and the lateral friction forces calculated from the parallel AIMD and DPMD simulations during the sliding at 1 GPa share the same dynamical behavior, fluctuating with very similar amplitudes on very similar time scales.

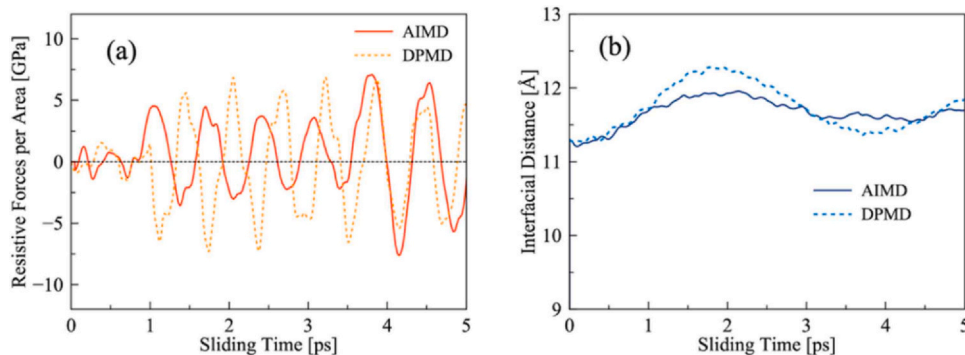


**Fig. 5.** Comparison of the resistive forces (a) and interfacial distance (b) predicted by DPMD and AIMD simulations of the sliding of the Fe-6BG system at 1 GPa and 300 K.

Overall, with a much lower computational cost, the BG-DNN15 potential has retained the DFT accuracy in all studied conditions.

A close comparison of AIMD vs DPMD and, together, vs ReaxFF is made possible by calculating the radial distribution functions (RDFs) of the most relevant atomic pairs. From Fig. 6a–b it is evident that there is an excellent agreement between AIMD and DPMD for the Fe-Fe RDFs and all the RDFs pairing C, O and H atoms from the BG molecules. For all the smaller valued RDFs pairing atoms at the interface (Fig. 6c), the first two peaks show again a very good agreement between the AIMD and the DPMD results, with only a very minor deviation at distances involving atoms far from the interface. Given the length of the simulations and the total number of atoms involved, the AIMD and DPMD RDFs are fully consistent within the associated statistical fluctuations, and we conclude that the BG-DNN15 potential accurately reproduces the underlying Fe-BG chemical interactions.

The Fe-O RDF first peaks at 2.25 Å (Fig. 6c), is suggesting that strong chemical bonds are formed between Fe and O atoms, in the expected range of Fe-O interfacial bonds. [65,66] As it can be seen in Fig. 6d–e, identical atomic configurations are established at the interface between Fe and BG molecules after the relaxation at 1 GPa both with DFT and with the BG-DNN15 potential. In marking contrast, the visually different atomic configuration in Fig. 6f is the one obtained when the interactions are described by the ReaxFF force field. The corresponding peak of the RDF for Fe-O pair is predicted at 3.02 Å by ReaxFF (Fig. 6c), which is too large value for supporting the possibility of Fe-O covalent bonds. Thus, with ReaxFF the main character of the the BG molecule adsorption on the Fe surface remains physical even under the relatively high 1 GPa load indicating that ReaxFF fails to describe accurately the tribochemical reaction consisting in the dissociation of O-H bonds and the formation of Fe-O bonds. After dissociating, the hydrogen atom also adsorbs on the Fe surface by forming Fe-H bonds (Fig. 6g–h), as it is demonstrated by the small peak centered at ~1.8 Å in the Fe-H RDF, which can be associated with the presence of a number of adsorbed hydrogen atoms. These results confirm that the BG-DNN15 potential correctly carries out the essential bonding information not only inside the BG molecular layer but also at the interface between Fe atoms and the BG molecules, while the selected ReaxFF model does not.

### 3.7. DPMD Simulations of tribological properties

DPMD simulations of the tribological performance of the butyl gallate monolayer were performed for systems containing 6, 54 and 72 molecules confined between two Fe substrates, with applied load pressures from 0.5 GPa up to 2.0 GPa. MD simulations for the smaller confined system (Fe-6BG) were started with the same setup pictured in Fig. 2e and used to run the initial ReaxFF MD and the DPMD simulations within the active learning process. The larger (Fe-54BG/Fe-72BG) systems were constructed with the same molecular geometry and

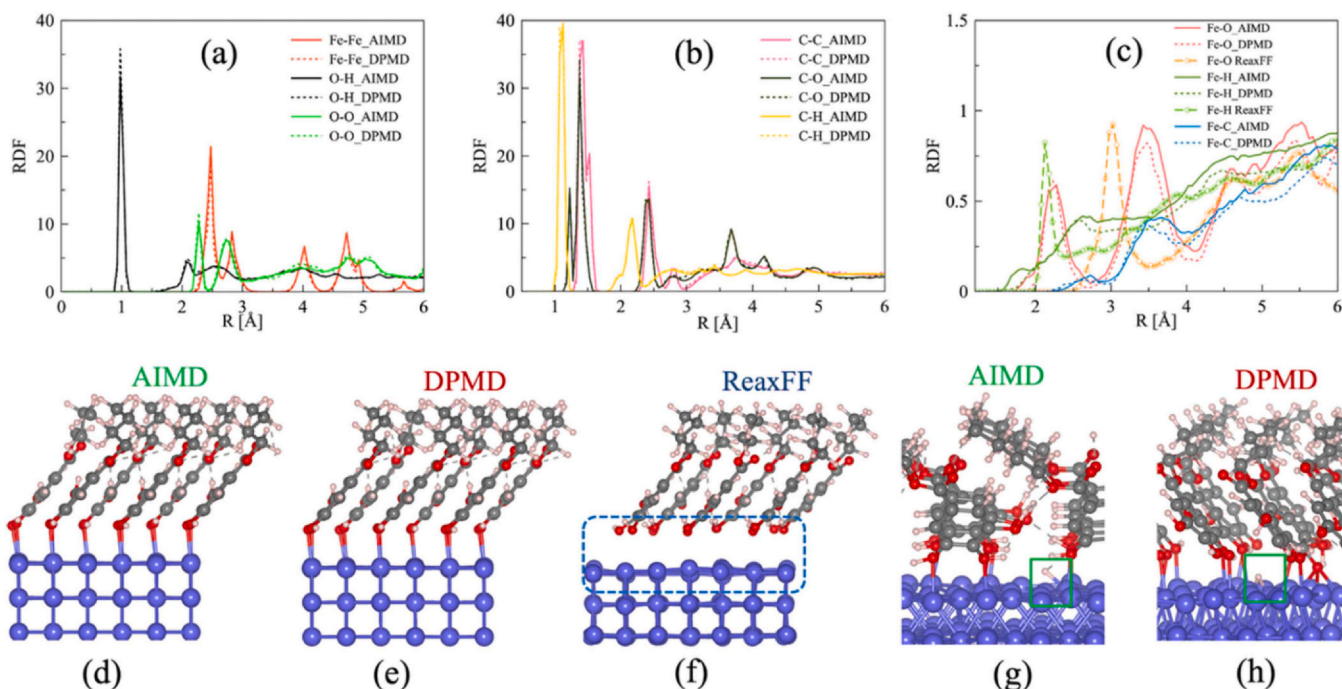


**Fig. 6.** (a–c) RDF of atomic pairs in the Fe–6BG system obtained during the thermalization at 300 K and 1 GPa for 4 (10) ps. Snapshots of the Fe–6BG configurations after the relaxation at 1 GPa by AIMD (d), DPMD (e), and ReaxFF (f). Snapshots of the OH bond dissociation and the Fe–H bond formation between at the Fe–BG interface during the thermalization of the Fe–6BG system at 1 GPa and 300 K: (g) by AIMD at 0.3 ps and (h) by DPMD at ~3 ps. In (d–h) snapshots the Fe atoms of the upper substrate have been removed for clarity and dashed lines show hydrogen bonding. Atom color codes as for Fig. 1.

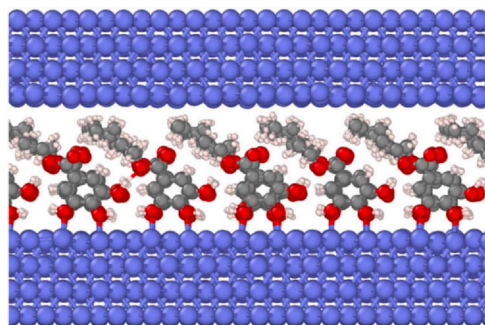


**Fig. 7.** A snapshot of the Fe-72BG system after relaxation at 1.0 GPa load where the BG SAM is stabilized by the Fe–O bond formation at the interface.

coverage and their dynamics integrated for long times in order to obtain a better statistic for the properties characterizing the frictional process. The 54 (72) BG molecules were distributed over the Fe (110) surface in a supercell with lateral dimensions 42.60 Å × 36.15 Å (42.60 Å × 48.20 Å). The size of the Fe-54BG (Fe-72BG) system corresponds to a number of atoms equal to 3780 (5040) in total, 2160 (2880) of which are Fe atoms (Fig. 7).

In order to impose a normal pressure with values of 0.5, 1.0, 1.5, and 2.0 GPa, a corresponding constant external vertical force was applied on each atom of the topmost atomic layer of the upper Fe slab, while keeping fixed the positions of the atoms of the bottom-most atomic layer of the lower Fe slab. Independent Nosé Hoover thermostats with a damping parameter of 10 fs were applied to the group of atoms forming the three inner layers of each Fe slabs with the same reference temperature  $T = 300$  K, while the temperature of the molecular layer was not controlled. Both systems were equilibrated for 100 ps under the applied load. After that, the dynamics under imposed lateral sliding with a velocity of the topmost Fe atoms fixed at 0.5 Å/ps was integrated for up to 1 ns of dynamics. For each system averages were taken, after reaching stationary conditions, on the final 600 ps of the dynamical trajectory under sliding in tribological conditions.

Fig. 8 a–c shows the dynamical behavior of the interfacial distance between the two Fe surfaces in each of the systems at three different load values. During the sliding, the interfacial distances, after an initial adjustment, fluctuate around a stable value, which is reached somewhat later for the systems at the higher 1.5 GPa and 2.0 GPa loads. Overall, the stability of the BG SAM layer is very well maintained up to the 2.0 GPa load.

The resistive, friction, force per atom was evaluated averaging the atomic forces on the iron atoms which were subjected to either velocity or position constraints, i.e. the topmost and the bottom-most Fe atoms. The values are converted to GPa units using the cell area. Fig. 8 d–f and Table 2 show that in the 0.5 – 2.0 GPa load range, thanks to the presence of the BG-molecule SAM anchored on the lower Fe surface, the friction force is dominated by the van der Waals interactions between the upper iron surface and the hydrocarbon chains of the BG molecules and is therefore reduced to very low values, compared to the case of bare Fe surfaces. The resistive forces increase slightly with increasing applied loads, while the opposite occurs for the interfacial separation between the two Fe slabs with decreasing  $\Delta z$  distances. Such decrease at higher loads in the separation between the two slabs, i.e., in the height of the SAM, accompanied by the friction increase is in an agreement with the general trends in tribological experiments.

The same tendencies were observed in the three different size systems. The average interfacial distance as a function of applied load shows an excellent agreement among the systems, with a maximum deviation in the  $\langle \Delta z \rangle$  of ~0.16 Å between the Fe-6BG and the Fe-54BG systems at 2 GPa (Table 2). The friction forces of the Fe-54BG and of the Fe-72BG systems are fully consistent between themselves for all loads, while the corresponding values are slightly higher for the Fe-6BG system, although still within the error bars which are relatively large for these smaller systems despite the long averaging simulation time. This result highlights the importance of using systems sizes large enough in the simulations, with increasing size much more effective than increasing time to obtain better statistics for the frictional properties.

Finally, the behavior of the Fe-54BG system was investigated to explore the effects of varying the applied sliding velocity. As it can be



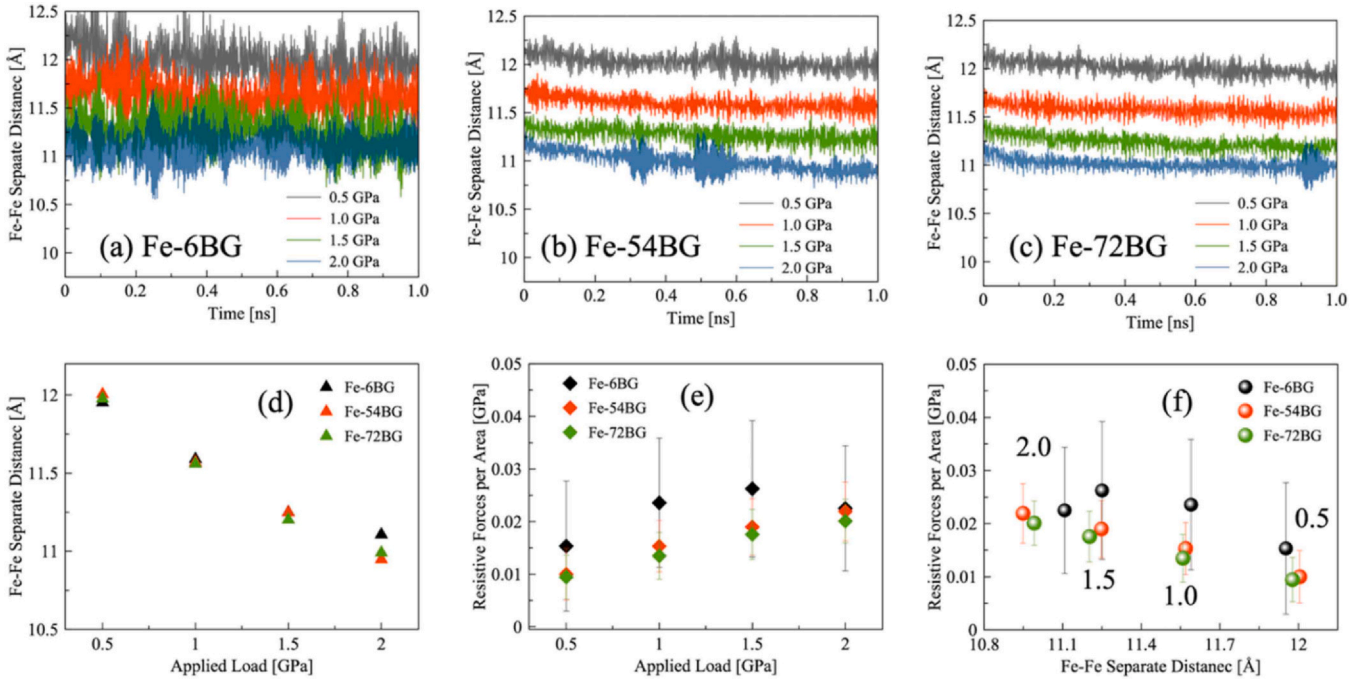


**Fig. 8.** Interfacial distance as a function of sliding time in Fe-6BG (a), Fe-54BG (b) and Fe-72BG (c) systems. Interfacial distance (d) and resistive force (e) as a function of applied load. The resistive force as a function of interfacial distance (f).

seen in Fig. 9 there is no significant dependence of the interfacial distance from the value of the imposed sliding velocity, a finding which is consistent with the contemporary only mild increase of the resistive forces at higher velocities. The system remains in the low friction conditions and show a consistent monotonic behavior with respect to the variation of the applied load at all values of the velocities. Table 3

#### 4. Discussion

To further investigate the structural changes in the system in response to tribological conditions, we have analyzed the RDFs of the interfacial atomic pairs, comparing the results separately collected in the first 20 ps of the thermalization and in the last 20 ps of the sliding, under loads of 1.0 GPa and 2.0 GPa. The results in Fig. 10 clearly shows structural changes associated with the modifications of the interfacial bonding which are represented by the different heights of the first peak of the RDFs. Particularly at 1.0 GPa, the peak at  $\sim 1.7$  Å in the Fe-H RDF is substantially enhanced, indicating the detachment of H atoms from the molecular OH bonds and their subsequent adsorption on the Fe surface. Particularly, one can see that at the same time the distance of the first peak in the Fe-O RDF decreases from  $\sim 2.17$  Å

to  $\sim 2.08$  Å, i.e. the OH bond dissociation is accompanied by the transformation of Fe-OH bonds into shorter Fe-O bonds, together with the establishment of Fe-O-C bridges. This process is in line with the DFT predicted result shown in Fig. 1c and plays a critical role to stabilize the SAM. [60] Finally at 2.0 GPa (Fig. 10b), one can observe a high degree of H dissociation and Fe-O-C bond formation already present during thermalization (Fig. 10c), indicating that the more severe condition facilitates OH dissociation. The sliding leads to a more pronounced presence of these events as shown by sharper peaks of Fe-O and Fe-H RDFs. Meanwhile, the Fe-C peaks remain almost unchanged up to 2 GPa, which confirms the stability of the SAM packing as upright configurations. In the one nanosecond simulations under sliding conditions, no Fe-O bond breaking was observed. This can be explained by the fact that the BG layer is chemisorbed onto the lower surface with stable Fe-O chemical bonds while there are only weaker van der Waals interactions between the hydrocarbon chains of the BG layer and the atoms of the upper iron surface. This weak interaction is not enough to make it probable in the given timeframe to observe Fe-O bond breaking at the lower surface, where the BG SAM is tightly packed adsorbed on the Fe substrate, leaving no vacant space for the molecules to move horizontally on the surface. This result confirms the stability of the BG SAM, which is an important feature for

**Table 2**

Results for the Fe-Fe separate distance  $\langle \Delta z \rangle$  between top and bottom iron layers, and the average friction force  $\langle F_x \rangle$  per area for Fe-6BG, Fe-54BG and Fe-72BG systems.

Load	$\langle \Delta z \rangle / \text{\AA}$			$\langle F_x \rangle / \text{GPa}$		
	Fe-6BG	Fe-54 BG	Fe-72BG	Fe-6BG	Fe-54 BG	Fe-72BG
0.5 GPa	11.952	12.005	11.977	0.015	0.010	0.009
1.0 GPa	11.590	11.569	11.559	0.024	0.015	0.013
1.5 GPa	11.250	11.248	11.202	0.026	0.019	0.018
2.0 GPa	11.107	10.949	10.991	0.023	0.022	0.020

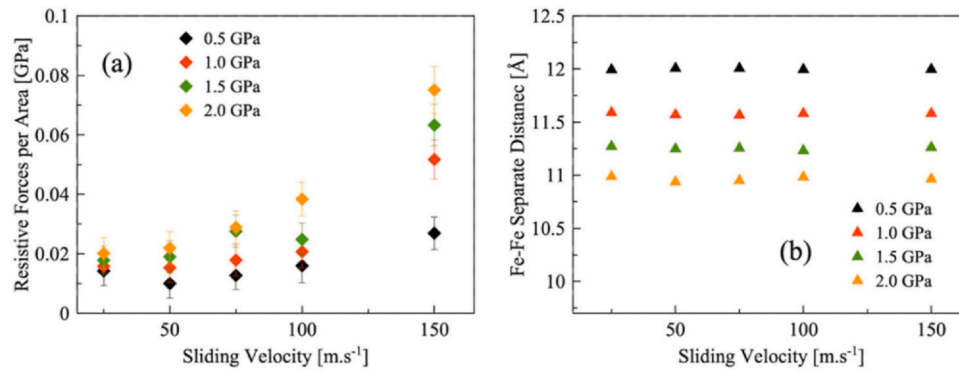


Fig. 9. (a) Average friction force  $\langle F_x \rangle$  per area and (b) Fe-Fe interfacial separations  $\langle \Delta z \rangle$  as a function of sliding velocity.

**Table 3**

Results for the Fe-Fe separate distance  $\langle \Delta z \rangle$  between top and bottom iron layers, and the average friction force  $\langle F_x \rangle$  per area as a function of sliding velocity for Fe-54BG system.

Load Velocity	$\langle \Delta z \rangle / \text{\AA}$				$\langle F_x \rangle / \text{GPa}$			
	0.5 GPa	1.0 GPa	1.5 GPa	2.0 GPa	0.5 GPa	1.0 GPa	1.5 GPa	2.0 GPa
25 [m/s]	11.992	11.589	11.270	10.936	0.014	0.016	0.018	0.020
50 [m/s]	12.005	11.569	11.248	10.949	0.010	0.015	0.019	0.022
75 [m/s]	12.004	11.566	11.254	10.982	0.013	0.018	0.028	0.029
100 [m/s]	11.994	11.581	11.231	10.963	0.016	0.020	0.025	0.038
150 [m/s]	11.995	11.581	11.261	10.993	0.027	0.052	0.063	0.075

friction reduction. Furthermore, on the longer times one can see the diffusion of detached hydrogen atoms into the Fe substrate (Fig. 10d), occurring under sliding conditions (see also Video S1 in the Supporting Information). However, the process only contributes with a minor effect on frictional properties which are governed by the interaction of the hydrocarbon tails with the upper Fe substrate. [62]

Supplementary material related to this article can be found online at [doi:10.1016/j.commt.2024.100005](https://doi.org/10.1016/j.commt.2024.100005).

In conclusion, in this work we show how, for the first time, a deep neural network potential has been trained to accurately describe, with the same “quantum accuracy” attained at the DFT level but with the

much lower computational cost of classical MD, the tribochemical dynamics of a model system in which a new class of eco-friendly lubricant, i.e. gallate molecules is used as an additive for reducing friction between two ideal iron surfaces sliding under load. One key aspect behind the efficiency as lubricant additive of the BG molecules unveiled by our simulations can be identified in the strong anchoring of the BG molecules to the iron surface which leads to the formation of strong Fe-O-C bridges made possible by hydrogen dissociation from OH bonds close to the iron surface. Hints at such a possibility came initially from our static DFT adsorption calculations and its enhancement in tribological conditions was duly confirmed by the extensive DPMD simulations with the

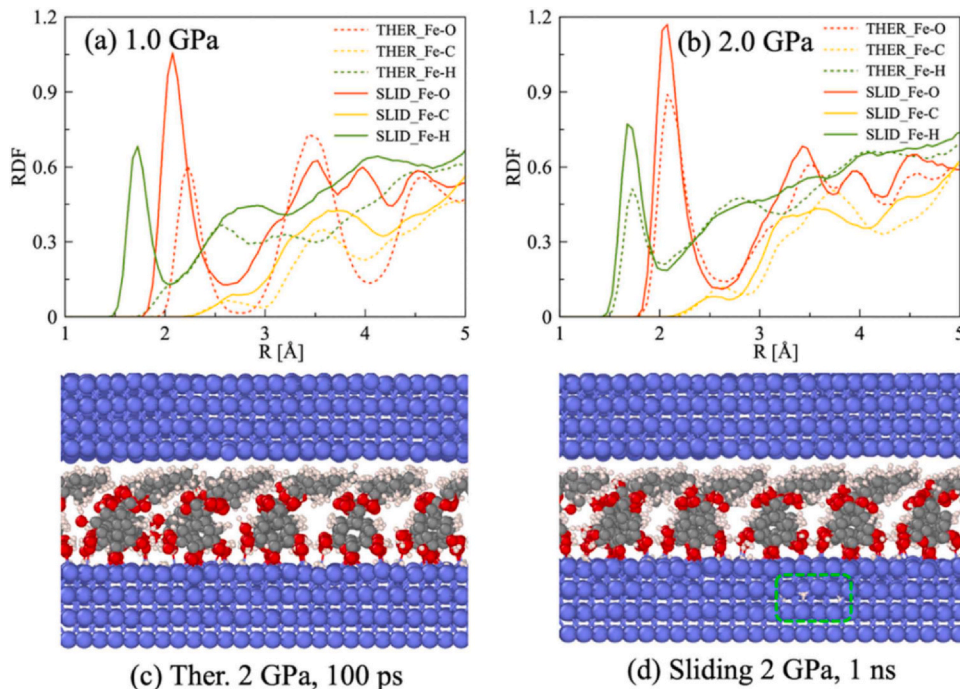


Fig. 10. RDF of interfacial pairs of the Fe-72BG system averaged during (a) the first 20 ps of thermalization and (b) the last 20 ps of the sliding at 1.0 and 2.0 GPa. (c) Snapshots of the configurations of the Fe-72BG system at 100 ps of the thermalization (c) and at 1 ns of the sliding at 2 GPa. The dotted green line in (d) highlights a region where hydrogen atoms are visible while diffusing into the Fe substrate.

trained NN potential model. On the contrary, we found that this mechanism simply cannot be reproduced in simulations using reactive force-fields as it does not occur even under harsh conditions in sliding simulations under loads. With such strong anchoring stabilizing the structure of the SAM, low friction arises from the resulting weak, mainly van der Waals, interactions between the hydrocarbon chains and the opposed iron surface.

To successfully train the BG-DNN15 potential model from *ab initio* data, it has been essential to include in the active learning procedure configurations generated under very harsh tribological conditions, and to perform a number of additional validation tests by direct comparison with AIMD simulations on a small-scale model system before conducting long time simulations with large system by DPMD using the trained potential model. Our work indicates that neural network-based potentials can be practically applied to study reactions in complex tribological systems, providing atomistic insights that can greatly enhance the comprehension of real-time experiments. We plan to expand the current BG-DNN15 model to explore the effects of the lubricant molecule chain length and the related mechanisms underlying friction and wear reductions for the gallate class of green lubricant additives.

### CRedit authorship contribution statement

**Maria Clelia Righi:** Writing – review & editing, Writing – original draft, Supervision, Investigation, Formal analysis, Conceptualization. **Huong T. T. Ta:** Writing – review & editing, Writing – original draft, Methodology, Investigation, Data curation. **Mauro Ferrario:** Writing – review & editing, Writing – original draft, Methodology, Investigation, Formal analysis, Data curation. **Sophie Loehlé:** Writing – review & editing, Writing – original draft, Methodology, Formal analysis, Conceptualization.

### Data availability

Data will be made available on request.

### Declaration of Competing Interest

The authors declare that they have no known competing financial interests or personal relationships that could have appeared to influence the work reported in this paper.

### Acknowledgments

We acknowledge the project “Advancing Solid Interface and Lubricants by First Principles Material Design (SLIDE)” that has received funding from the European Research Council (ERC) under the “European Union’s Horizon 2020 research and innovation program (Grant agreement No. 865633)”. We acknowledge the CINECA award IscrC\_AM-SLUB under the ISCRA initiative, for the availability of high-performance computing resources and support.

### Appendix A. Supporting information

Supplementary data associated with this article can be found in the online version at [doi:10.1016/j.commt.2024.100005](https://doi.org/10.1016/j.commt.2024.100005).

### References

- [1] A.A.L. Michalchuk, E.V. Boldyreva, A.M. Belenguer, F. Emmerling, V.V. Boldyrev, Tribochemistry, mechanical alloying, mechanochemistry: what is in a name? *Front. Chem.* 9 (2021) 685789, <https://doi.org/10.3389/fchem.2021.685789>.
- [2] S.M. Hsu, J. Zhang, Z. Yin, The nature and origin of tribochemistry, *Tribol. Lett.* 23 (2002) 131–139, <https://doi.org/10.1023/A:1020112901674>.
- [3] Z.R. Zhou, Z.M. Jin, Biotribology: recent progresses and future perspectives, *Biosurf. Biotribol.* 1 (1) (2015) 3–24, <https://doi.org/10.1016/j.bsbt.2015.03.001>.
- [4] E. Serpini, A. Rota, S. Valeri, E. Ukraintsev, B. Rezek, T. Polcar, P. Nicolini, Nanoscale frictional properties of ordered and disordered MoS<sub>2</sub>, *Tribol. Int* 136 (2019) 67–74, <https://doi.org/10.1016/j.triboint.2019.03.004>.
- [5] B. Bhushan, Nanotribology and nanomechanics of MEMS/NEMS and BioMEMS/BioNEMS materials and devices, *Micro Eng.* 84 (3) (2007) 387–412, <https://doi.org/10.1016/j.mee.2006.10.059>.
- [6] H. Jiang, X. Hou, Y. Ma, D. Su, Y. Qian, M.K. Ahmed Ali, K.D. Dearn, The tribological performance evaluation of steel-steel contact surface lubricated by poly-alphaolefins containing surfactant-modified hybrid MoS<sub>2</sub>/h-BN nano-additives, *Wear* 504–505 (2022) 204426, <https://doi.org/10.1016/j.wear.2022.204426>.
- [7] K. Feng, J. Ni, Z. Wang, Z. Meng, Tribological properties of high-speed steel surface with texture and vertical fibers, *Sci. Rep.* 13 (1) (2023) 13180, <https://doi.org/10.1038/s41598-023-39721-2>.
- [8] A.A. Voevodin, J.P. O'Neill, J.S. Zabinski, Nanocomposite tribological coatings for aerospace applications, *Surf. Coat. Tech.* 116 (1999) 36–45 ([www.elsevier.nl/locate/surfcoat](http://www.elsevier.nl/locate/surfcoat)).
- [9] A.A. Voevodin, J.P. O'Neill, J.S. Zabinski, WC/DLC/WS<sub>2</sub> Nanocomposite coatings for aerospace tribology, *Tribol. Lett.* 6 (1999) 75–79.
- [10] H. Carlton, D. Huitink, H. Liang, Tribochemistry as an Alternative Synthesis Pathway, *Lubricants* 8 (2020) 87, <https://doi.org/10.3390/LUBRICANTS8090087>.
- [11] H.T.T. Ta, N.V. Tran, A.K. Tieu, H. Zhu, H. Yu, T.D. Ta, Computational tribochemistry: a review from classical and quantum mechanics studies, *J. Phys. Chem. C* (2021) 16875–16891, <https://doi.org/10.1021/acs.jpcc.1c03725>.
- [12] A.I. Vakis, V.A. Yastrebov, J. Scheibert, L. Nicola, D. Dini, C. Minfray, A. Almqvist, M. Paggi, S. Lee, G. Limbert, J.F. Molinari, G. Anciaux, R. Aghababaei, S. Echeverri Restrepo, A. Papangelo, A. Cammarata, P. Nicolini, C. Putignano, G. Carbone, S. Stupkiewicz, J. Lengiewicz, G. Costagliola, F. Bosia, R. Guarino, N.M. Pugno, M.H. Müser, M. Ciavarella, Modeling and simulation in tribology across scales: an overview, *Tribology Int.* (2018) 169–199, <https://doi.org/10.1016/j.triboint.2018.02.005>.
- [13] S. Loehlé, M.C. Righi, Ab initio molecular dynamics simulation of tribochemical reactions involving phosphorus additives at sliding iron interfaces, *Lubricants* 6 (2) (2018), <https://doi.org/10.3390/lubricants6020031>.
- [14] H.T.T. Ta, A.K. Tieu, H. Zhu, H. Yu, N.V. Tran, B.H. Tran, S. Wan, T.D. Ta, Ab initio study on physical and chemical interactions at borates and iron oxide interface at high temperature, *Chem. Phys.* 529 (2020), <https://doi.org/10.1016/j.chemphys.2019.110548>.
- [15] N.V. Tran, A. Kiet Tieu, H. Zhu, H.T.T. Ta, P.T. Sang, H.M. Le, T.D. Ta, Insights into the tribochemistry of sliding iron oxide surfaces lubricated by sodium silicate glasses: an Ab initio molecular dynamics study, *Appl. Surf. Sci.* 528 (2020), <https://doi.org/10.1016/j.apsusc.2020.147008>.
- [16] C.J. Carkner, N.J. Mosey, Slip mechanisms of hydroxylated  $\alpha$ -Al<sub>2</sub>O<sub>3</sub> (0001)/(0001) interfaces: a first-principles molecular dynamics study, *J. Phys. Chem. C* 114 (41) (2010) 17709–17719, <https://doi.org/10.1021/jp1055478>.
- [17] C.J. Carkner, S.M. Haw, N.J. Mosey, Effect of adhesive interactions on static friction at the atomic scale, *Phys. Rev. Lett.* 105 (5) (2010), <https://doi.org/10.1103/PhysRevLett.105.056102>.
- [18] M.I. De Barros Bouchet, G. Zilibotti, C. Matta, M.C. Righi, L. Vandenbulcke, B. Vacher, J.M. Martin, Friction of diamond in the presence of water vapor and hydrogen gas. Coupling gas-phase lubrication and first-principles studies, *J. Phys. Chem. C* 116 (12) (2012) 6966–6972, <https://doi.org/10.1021/jp211322s>.
- [19] H.T.T. Ta, N.V. Tran, M.C. Righi, Nanotribological properties of oxidized diamond/silica interfaces: insights into the atomistic mechanisms of wear and friction by Ab initio molecular dynamics simulations, *ACS Appl. Nano Mater.* 6 (18) (2023) 16674–16683, <https://doi.org/10.1021/acsnanm.3c02881>.
- [20] M. Cutini, G. Forghieri, M. Ferrario, M.C. Righi, Adhesion, friction and tribochemical reactions at the diamond–silica interface, *Carbon* 203 (2023) 601–610, <https://doi.org/10.1016/j.carbon.2022.11.074>.
- [21] M. Cutini, G. Forghieri, M. Ferrario, M.C. Righi, Adhesion, friction and tribochemical reactions at the diamond–silica interface, *Carbon* 203 (2023) 601–610, <https://doi.org/10.1016/j.carbon.2022.11.074>.
- [22] T. Onodera, Y. Morita, A. Suzuki, R. Sahnoun, M. Koyama, H. Tsuboi, N. Hatakeyama, A. Endou, H. Takaba, M. Kubo, C.A. Del Carpio, C. Minfray, J.M. Martin, A. Miyamoto, A theoretical investigation on the abrasive wear prevention mechanism of ZDDP and ZP tribofilms, *Appl. Surf. Sci.* 254 (23) (2008) 7976–7979, <https://doi.org/10.1016/j.apsusc.2008.04.057>.
- [23] J.M. Martin, T. Onodera, M.I. De Barros Bouchet, N. Hatakeyama, A. Miyamoto, Anti-wear chemistry of ZDDP and calcium borate nano-additive. Coupling experiments, chemical hardness predictions, and MD calculations, *Tribol. Lett.* 50 (1) (2013) 95–104, <https://doi.org/10.1007/s11249-013-0108-z>.
- [24] A. Li, Y. Liu, I. Szlufarska, Effects of interfacial bonding on friction and wear at silica/silica interfaces, *Tribol. Lett.* 56 (3) (2014) 481–490, <https://doi.org/10.1007/s11249-014-0425-x>.
- [25] D.C. Yue, T.B. Ma, Y.Z. Hu, J. Yeon, A.C.T. Van Duin, H. Wang, J. Luo, Tribochemistry of phosphoric acid sheared between quartz surfaces: a reactive molecular dynamics study, *J. Phys. Chem. C* 117 (48) (2013) 25604–25614, <https://doi.org/10.1021/jp406360u>.
- [26] T.D. Ta, H.M. Le, A.K. Tieu, H. Zhu, H.T.T. Ta, N.V. Tran, S. Wan, A. van Duin, Reactive molecular dynamics study of hierarchical tribochemical lubricant films at elevated temperatures, *ACS Appl. Nano Mater.* 3 (3) (2020) 2687–2704, <https://doi.org/10.1021/acsnanm.0c00042>.
- [27] D.C. Yue, T.B. Ma, Y.Z. Hu, J. Yeon, A.C.T. Van Duin, H. Wang, J. Luo, Tribochemical mechanism of amorphous silica asperities in aqueous environment: a reactive molecular dynamics study, *Langmuir* 31 (4) (2015) 1429–1436, <https://doi.org/10.1021/la5042663>.
- [28] J. Wen, T. Ma, W. Zhang, G. Psogianakis, A.C.T. van Duin, L. Chen, L. Qian, Y. Hu, X. Lu, Atomic insight into tribochemical wear mechanism of silicon at the Si/SiO<sub>2</sub> interface in aqueous environment: molecular dynamics simulations using ReaxFF reactive force field, *Appl. Surf. Sci.* 390 (2016) 216–223, <https://doi.org/10.1016/j.apsusc.2016.08.082>.



- [29] J. Yeon, A.C.T. Van Duin, S.H. Kim, Effects of water on tribochemical wear of silicon oxide interface: molecular dynamics (MD) study with reactive force field (ReaxFF), *Langmuir* 32 (4) (2016) 1018–1026, <https://doi.org/10.1021/acs.langmuir.5b04062>.
- [30] A. Peguiron, G. Moras, M. Walter, H. Uetsuka, L. Pastewka, M. Moseler, Activation and mechanochemical breaking of C-C bonds initiate wear of diamond (110) surfaces in contact with silica, *Carbon* 98 (2016) 474–483, <https://doi.org/10.1016/j.carbon.2015.10.098>.
- [31] Z. Shi, Z. Jin, X. Guo, S. Yuan, J. Guo, Insights into the Atomistic Behavior in Diamond Chemical Mechanical Polishing with [Rad]OH Environment Using ReaxFF Molecular Dynamics Simulation, *Comput. Mater. Sci.* 166 (2019) 136–142, <https://doi.org/10.1016/j.commatsci.2019.05.001>.
- [32] J. Behler, M. Parrinello, Generalized neural-network representation of high-dimensional potential-energy surfaces, *Phys. Rev. Lett.* 98 (14) (2007), <https://doi.org/10.1103/PhysRevLett.98.146401>.
- [33] A.P. Bartók, M.C. Payne, R. Kondor, G. Csányi, Gaussian approximation potentials: the accuracy of quantum mechanics, without the electrons, *Phys. Rev. Lett.* 104 (13) (2010), <https://doi.org/10.1103/PhysRevLett.104.136403>.
- [34] S. Chmiela, A. Tkatchenko, H.E. Sauceda, I. Poltavsky, K.T. Schütt, K.-R. Müller, Machine learning of accurate energy-conserving molecular force fields, *Sci. Adv.* 3 (2017) e160301 (<https://www.science.org>).
- [35] H. Wang, Z. Zhang, J. Han, DeepPMD-kit: a deep learning package for many-body potential energy representation and molecular dynamics, *Comput. Phys. Commun.* 228 (2018) 178–184, <https://doi.org/10.17632/hvfh9yvncl.1>.
- [36] Y. Deng, C. Wang, X. Xu, H. Li, Machine learning potential for Ab initio phase transitions of zirconia, *Theor. Appl. Mech. Lett.* (2023) 100481, <https://doi.org/10.1016/j.taml.2023.100481>.
- [37] X. Wang, Z. Zhang, P. Gao, C. Zhang, J. Lv, H. Wang, H. Liu, Y. Wang, Y. Ma, Data-driven prediction of complex crystal structures of dense lithium, *Nat. Commun.* 14 (1) (2023), <https://doi.org/10.1038/s41467-023-38650-y>.
- [38] Y. Cheng, H. Wang, S. Wang, X. Gao, Q. Li, J. Fang, H. Song, W. Chu, G. Zhang, H. Song, H. Liu, Deep-learning potential method to simulate shear viscosity of liquid aluminum at high temperature and high pressure by molecular dynamics, *AIP Adv.* 11 (1) (2021), <https://doi.org/10.1063/5.0036298>.
- [39] L. Zhang, G. Csányi, E. van der Giessen, F. Maresca, Atomistic fracture in Bcc iron revealed by active learning of Gaussian approximation potential, *NPJ Comput. Mater.* 9 (1) (2023), <https://doi.org/10.1038/s41524-023-01174-6>.
- [40] J. Zeng, L. Zhang, H. Wang, T. Zhu, Exploring the chemical space of linear alkane pyrolysis via deep potential generator, *Energy Fuels* 35 (1) (2021) 762–769, <https://doi.org/10.1021/acs.energyfuels.0c03211>.
- [41] Designed Research; T., P.G.D.E.G.; Performed Research; T., P. M. P. E. G Signatures of a Liquid-Liquid Transition in an Ab Initio Deep Neural Network Model for Water. 2020, 117, 26040–26046. <https://doi.org/10.1073/pnas.2015440117/-DCSupplemental>.
- [42] M.F.C. Andrade, H.Y. Ko, L. Zhang, R. Car, A. Selloni, Free energy of proton transfer at the water-TiO<sub>2</sub> interface from: ab initio deep potential molecular dynamics, *Chem. Sci.* 11 (9) (2020) 2335–2341, <https://doi.org/10.1039/c9sc05116c>.
- [43] Z. Li, X. Tan, Z. Fu, L. Liu, J.Y. Yang, Thermal transport across copper-water interfaces according to deep potential molecular dynamics, *Phys. Chem. Chem. Phys.* 25 (9) (2023) 6746–6756, <https://doi.org/10.1039/d2cp05530a>.
- [44] X.T. Fan, X.J. Wen, Zhuang, Y. Bin, J. Cheng, Molecular insight into the GaP (110)–water interface using machine learning accelerated molecular dynamics, *J. Energy Chem.* 82 (2023) 239–247, <https://doi.org/10.1016/j.jechem.2023.03.013>.
- [45] M. De La Puente, R. David, A. Gomez, D. Laage, Acids at the edge: why nitric and formic acid dissociations at air-water interfaces depend on depth and on interface specific area, *J. Am. Chem. Soc.* 144 (23) (2022) 10524–10529, <https://doi.org/10.1021/jacs.2c03099>.
- [46] Y. Zhang, H. Huang, J. Tian, C. Li, Y. Jiang, Z. Fan, L. Pan, Modelling electrified microporous carbon/electrolyte electrochemical interface and unraveling charge storage mechanism by machine learning accelerated molecular dynamics, *Energy Storage Mater.* 63 (2023) 103069, <https://doi.org/10.1016/j.ensm.2023.103069>.
- [47] Y. Bin Zhuang, J. Cheng, Deciphering the anomalous acidic tendency of terminal water at rutile(110)-water interfaces, *J. Phys. Chem. C* 127 (22) (2023) 10532–10540, <https://doi.org/10.1021/acs.jpcc.3c01870>.
- [48] C. Hu, J. Ai, L. Ma, P. Wen, M. Fan, F. Zhou, W. Liu, Ester oils prepared from fully renewable resources and their lubricant base oil properties, *ACS Omega* (2021), <https://doi.org/10.1021/acsomega.1c00808>.
- [49] S. Loehlé, C. Matta, C. Minfray, T. Le Mogne, R. Iovine, Y. Obara, A. Miyamoto, J.M. Martin, Mixed lubrication of steel by C18 fatty acids revisited. Part II: influence of some key parameters, *Tribol. Int.* 94 (2016) 207–216, <https://doi.org/10.1016/j.triboint.2015.08.036>.
- [50] G. Kresse, J. Furthmüller, Efficient iterative schemes for ab initio total-energy calculations using a plane-wave basis set, *Phys. Rev. B* 54 (1996) 11169, <https://doi.org/10.1103/PhysRevB.54.11169>.
- [51] J.P. Perdew, K. Burke, M. Ernzerhof, Generalized gradient approximation made simple, *Phys. Rev. Lett.* 77 (1996) 3865, <https://doi.org/10.1103/PhysRevLett.77.3865>.
- [52] S. Grimme, Semiempirical GGA-type density functional constructed with a long-range dispersion correction, *J. Comput. Chem.* 27 (15) (2006) 1787–1799, <https://doi.org/10.1002/jcc.20495>.
- [53] T. Bučko, J. Hafner, S. Lebègue, J.G. Ángyán, Improved description of the structure of molecular and layered crystals: Ab initio DFT calculations with van Der Waals corrections, *J. Phys. Chem. A* 114 (43) (2010) 11814–11824, <https://doi.org/10.1021/jp106469x>.
- [54] G. Zilibotti, S. Corni, M.C. Righi, Load-induced confinement activates diamond lubrication by water, *Phys. Rev. Lett.* 111 (14) (2013) 146101, <https://doi.org/10.1103/PhysRevLett.111.146101>.
- [55] S. Plimpton, Fast parallel algorithms for short-range molecular dynamics, *J. Comp. Phys.* 117 (1995) 1–19, <https://doi.org/10.1006/jcph.1995.1039>.
- [56] Y.K. Shin, H. Kwak, A.V. Vasenkov, D. Sengupta, A.C.T. Van Duin, Development of a ReaxFF reactive force field for Fe/Cr/O/S and application to oxidation of butane over a pyrite-covered Cr<sub>2</sub>O<sub>3</sub> catalyst, *ACS Catal.* 5 (12) (2015) 7226–7236, <https://doi.org/10.1021/acscatal.5b01766>.
- [57] H. Wang, X. Guo, L. Zhang, H. Wang, J. Xue, Deep learning inter-atomic potential model for accurate irradiation damage simulations, *Appl. Phys. Lett.* 114 (24) (2019), <https://doi.org/10.1063/1.5098061>.
- [58] M. Abadi, P. Barham, J. Chen, Z. Chen, A. Davis, J. Dean, M. Devin, S. Ghemawat, G. Irving, M. Isard, M. Kudlur, J. Levenberg, R. Monga, S. Moore, D.G. Murray, B. Steiner, P. Tucker, V. Vasudevan, P. Warden, M. Wicke, Y. Yu, X. Zheng, TensorFlow: a system for large-scale machine learning, In *Proceedings of the 12th USENIX Conference on Operating Systems Design and Implementation*; OSDI'16, USENIX Association, USA, 2016, pp. 265–283.
- [59] Y. Zhang, H. Wang, W. Chen, J. Zeng, L. Zhang, H. Wang, DP-GEN: a concurrent learning platform for the generation of reliable deep learning based potential energy models, *Comput. Phys. Commun.* 253 (2020) 107206, <https://doi.org/10.17632/sxybkge5xc.1>.
- [60] C. Gattinoni, J.P. Ewen, D. Dini, Adsorption of surfactants on  $\alpha$ -Fe<sub>2</sub>O<sub>3</sub>(0001): a density functional theory study, *J. Phys. Chem. C* 122 (36) (2018) 20817–20826, <https://doi.org/10.1021/acs.jpcc.8b05899>.
- [61] M.H. Wood, M.T. Casford, R. Steitz, A. Zarbakhsh, R.J.L. Welbourn, S.M. Clarke, Comparative adsorption of saturated and unsaturated fatty acids at the iron oxide/oil interface, *Langmuir* 32 (2) (2016) 534–540, <https://doi.org/10.1021/acs.langmuir.5b04435>.
- [62] Y. Long, J. Galipaud, V. Wehnacht, S. Makowski, J.M. Martin, M.I. De Barros Bouchet, Achieving superlubricity using selected tribo-pairs lubricated by castor oil and unsaturated fatty acids, *Tribol. Int.* 169 (2022), <https://doi.org/10.1016/j.triboint.2022.107462>.
- [63] A. Mondal, D. Kussainova, S. Yue, A.Z. Panagiotopoulos, Modeling chemical reactions in alkali carbonate-hydroxide electrolytes with deep learning potentials, *J. Chem. Theory Comput.* 19 (14) (2023) 4584–4595, <https://doi.org/10.1021/acs.jctc.2c00816>.
- [64] Y.K. Shin, H. Kwak, A.V. Vasenkov, D. Sengupta, A.C.T. Van Duin, Development of a ReaxFF reactive force field for Fe/Cr/O/S and application to oxidation of butane over a pyrite-covered Cr<sub>2</sub>O<sub>3</sub> catalyst, *ACS Catal.* 5 (12) (2015) 7226–7236, <https://doi.org/10.1021/acscatal.5b01766>.
- [65] L. Guo, C. Qi, X. Zheng, R. Zhang, X. Shen, S. Kaya, Toward Understanding the adsorption mechanism of large size organic corrosion inhibitors on an Fe(110) surface using the DFTB method, *RSC Adv.* 7 (46) (2017) 29042–29050, <https://doi.org/10.1039/c7ra04120a>.
- [66] H.T.T. Ta, A.K. Tieu, H. Zhu, H. Yu, T.D. Ta, S. Wan, N.V. Tran, H.M. Le, Chemical origin of sodium phosphate interactions on iron and iron oxide surfaces by first principle calculations, *J. Phys. Chem. C* 122 (1) (2018) 635–647, <https://doi.org/10.1021/acs.jpcc.7b10731>.